



Short communication

Na₂V₆O₁₆·0.14H₂O nanowires as a novel anode material for aqueous rechargeable lithium battery with good cycling performance

Donghui Zhou, Suqin Liu*, Haiyan Wang*, Guiqing Yan

Key Laboratory of Resources Chemistry of Nonferrous Metals, Ministry of Education, School of Chemistry and Chemical Engineering, Central South University, Changsha, Hunan 410083, PR China

H I G H L I G H T S

- ▶ A novel anode material, Na₂V₆O₁₆·0.14H₂O nanowire was first proposed for aqueous lithium-ion battery.
- ▶ The effect of pH value of the electrolyte on electrochemical behavior of Na₂V₆O₁₆·0.14H₂O was optimized.
- ▶ ARLB of Na₂V₆O₁₆·0.14H₂O//LiMn₂O₄ was constructed and showed good electrochemical performance.

A R T I C L E I N F O

Article history:

Received 16 August 2012

Received in revised form

4 November 2012

Accepted 9 November 2012

Available online 17 November 2012

Keywords:

Aqueous rechargeable lithium battery

Anode

Sodium hexavanadate nanowires

Cycling stability

A B S T R A C T

The development of aqueous rechargeable lithium battery (ARLB) is greatly restricted by the anode material. Herein, Na₂V₆O₁₆·0.14H₂O nanowires with high cycling stability in the aqueous solution are firstly proposed as a novel anode material for ARLB. The effect of pH value of the electrolyte on electrochemical behavior of Na₂V₆O₁₆·0.14H₂O is optimized. The CV results demonstrate that the studied electrode possesses high reversible lithium insertion/extraction ability and it is more stable in neutral solution. The ARLB consisting of LiMn₂O₄ as cathode, Na₂V₆O₁₆·0.14H₂O as anode and saturated Li₂SO₄ as electrolyte indicates good cycling stability. An initial specific discharge capacity of 122.7 mAh g^{−1} (based on the mass of anode material) can be reached at 60 mA g^{−1}. The capacity retention is up to 80.1% and 77% of the initial discharge capacity at 300 mA g^{−1} after 100 and 200 cycles, respectively. The good cycling performance of the ARLB is partially due to suppression of the charge-transfer resistance.

© 2012 Elsevier B.V. All rights reserved.

1. Introduction

Nowadays, Li-ion batteries with organic electrolyte have been widely used in portable electronic devices. However, certain drawbacks such as safety issues at abuse conditions, high cost and rigorous operating requirements have greatly limited the further applications, particularly in electric vehicle (EV) and hybrid electric vehicle (HEV) [1,2]. An alternative rechargeable Li-ion battery with an aqueous electrolyte was first reported by Dahn and co-workers in 1994. Compared with non-aqueous lithium-ion battery, the safety problem is fundamentally settled, and rigorous assembly conditions can be also avoided. Additionally, ARLB uses a weak alkaline or neutral aqueous solution as the electrolyte, which is more environmental friendly [3–7]. Therefore, ARLB and related materials have attracted much attention in the field of electrochemical energy storage owing to its high safety, low cost,

environmental friendliness, and relatively high energy and power densities [8,9].

Note that the electrode reaction of lithium-ion intercalation compounds in aqueous electrolytes is far more complex than that in organic electrolyte. The hydrogen and oxygen evolution reactions must be taken into consideration. Therefore, selection of appropriate intercalation cathode and anode materials with proper Li-ion insertion/extraction potential and high discharge capacity as well as long cyclic performance is a key access to ARLB with high energy density and excellent cyclic stability [10]. It is verified that well-used cathode materials in organic lithium-ion battery such as LiCoO₂, LiNi_{1/3}Co_{1/3}Mn_{1/3}O₂, LiMn₂O₄, LiFePO₄ etc [4,11–13] could be used as cathode materials for ARLB. On the contrary, there are relatively less suitable anode materials for ARLB due to the limit of suitable lithium intercalation potential. Vanadium oxides and its derivatives have been widely studied for ARLB due to their high capacity, suitable voltage, and excellent kinetics resulting from their layered structure. Of these, LiV₃O₈ is the most studied one [14–16]. However, recent researches implied that rapid capacity fading of LiV₃O₈ was discovered during cycling in aqueous

* Corresponding authors. Tel./fax: +86 0731 88879850.

E-mail addresses: sqliu2003@126.com (S. Liu), wanghy419@126.com (H. Wang).

electrolyte probably due to V-dissolution and deterioration of the crystal structure [17,18]. Despite the fact that much work has devoted, the poor cycling stability of ARLB systems is still a big challenge, in which the anode materials are considered to play a vital role. Accordingly, it is of great importance to design a novel, high performance anode material to further better the cycling stability of the ARLB.

In our previous work, $\text{Na}_2\text{V}_6\text{O}_{16} \cdot x\text{H}_2\text{O}$ nanowires were synthesized by a facile method and first used as a cathode material in lithium-ion battery, which exhibited an initial discharge capacity of 189.2 mAh g^{-1} at 30 mA g^{-1} and no capacity fading at 300 mA g^{-1} over 100 cycles [19]. It is believed that the structure stability of annealed $\text{Na}_2\text{V}_6\text{O}_{16} \cdot x\text{H}_2\text{O}$ is much better than LiV_3O_8 and the V-dissolution could be effectively restricted due to its stable structure [19]. Moreover, like LiV_3O_8 , $\text{Na}_2\text{V}_6\text{O}_{16} \cdot x\text{H}_2\text{O}$ has the similar lithium intercalation potential. Recently, $\text{Na}_{0.33}\text{V}_2\text{O}_5$ was first introduced by Xie and co-workers [20] to be a high performance anode material. They considered that the improvement of ARLB was attributed to the crystallographical “pillar effect”, which could prevent the structure collapse and crystallinity loss during the lithium extraction/insertion process. Despite that the reversible capacity of sodium trivanadate is lower in comparison with lithium trivanadate, its cycling stability, as well proved, is much better due to unique structure [21,22]. Information above gives us inspiration that $\text{Na}_2\text{V}_6\text{O}_{16} \cdot x\text{H}_2\text{O}$ nanowires seem to be an appealing candidate for desirable anode material. In the present work, the electrochemical behavior of $\text{Na}_2\text{V}_6\text{O}_{16} \cdot 0.14\text{H}_2\text{O}$ nanowires in saturated Li_2SO_4 solution is well investigated and the new $\text{Na}_2\text{V}_6\text{O}_{16} \cdot 0.14\text{H}_2\text{O} // \text{LiMn}_2\text{O}_4$ system is constructed, which delivers good cycling stability with the capacity retention of 77% over 200 cycles at 300 mA g^{-1} . This work indicates that annealed $\text{Na}_2\text{V}_6\text{O}_{16} \cdot x\text{H}_2\text{O}$ nanowires could be used as a very promising anode material for ARLB.

2. Experimental

2.1. Synthesis and characterization of $\text{Na}_2\text{V}_6\text{O}_{16} \cdot 0.14\text{H}_2\text{O}$

$\text{Na}_2\text{V}_6\text{O}_{16} \cdot 0.14\text{H}_2\text{O}$ was prepared according to our earlier work [19]. All the starting materials were analytically pure grade and used as received. At first, 1.819 g of V_2O_5 and 0.400 g of NaOH were added to deionized water successively. The mixed solution was heated under magnetic stirring until it was dissolved. After stirring for 30 min, the suspension was transferred to 50 ml Teflon lined stainless steel autoclave. The total volume of the solution was about 40 ml. The autoclave was sealed and heated at 180°C for 48 h and allowed to cool to room temperature. The obtained precipitates were filtered, washed with deionized water several times, and then dried at 80°C overnight. For improving the cycling stability, the as-prepared products were further heated at 400°C for 2 h in air.

X-ray diffraction (XRD) data were performed using a Rigaku D/max2550VB⁺18 kW using graphite-monochromatized $\text{Cu K}\alpha$ radiation (40 kV, 250 mA). Morphology of the as-prepared material was investigated by a JSM6430F scanning electron microscopy (SEM). Fourier transform infrared (FT-IR) spectrum was recorded using Nicolet AVATAR560 FT-IR spectrometer. Thermal gravimetry (TGA) was carried out with a TA-SDTQ600 differential scanning calorimeter under N_2 atmosphere at a ramping rate of $10^\circ\text{C min}^{-1}$. The element analysis was determined by Baird ICP-AES spectrometer.

2.2. The preparation of the electrolyte

64 g Li_2SO_4 and 0.124 g $\text{LiOH} \cdot \text{H}_2\text{O}$ were dissolved in deionized water successively. The mixed solution was then transferred to 250 ml volumetric flask to obtaining the saturated electrolyte with

pH = 12, and the electrolytes with pH = 11 and pH = 9 were obtained similarly. The neutral solution was prepared without $\text{LiOH} \cdot \text{H}_2\text{O}$.

2.3. Electrochemical measurements

The used LiMn_2O_4 was provided by Hunan Reshine New Material Co., Ltd. The $\text{Na}_2\text{V}_6\text{O}_{16} \cdot 0.14\text{H}_2\text{O}$ and LiMn_2O_4 electrodes were made in a similar way. Test electrodes were fabricated by pressing a mixture of the sample, conductive material (acetylene black, AB), and binder (PTFE) in a weight ratio of 80:10:10 on a stainless steel mesh current collector at 20 MPa firstly and then dried at 110°C for 8 h. Half cell experiment was done via employing test electrodes as working electrode, combining with the platinum sheet electrode and saturated calomel reference electrode to form a three electrode system. Cyclic voltammetry was investigated at room temperature using an electrochemical station (CHI 660B). As follows, the electrochemical cells were constructed by using LiMn_2O_4 electrode as cathode, $\text{Na}_2\text{V}_6\text{O}_{16} \cdot 0.14\text{H}_2\text{O}$ electrode as anode, saturated Li_2SO_4 as electrolyte, assembling into CR2016 coin-type cells. Charge and discharge measurements of batteries were conducted under a desired current density by a Land CT2001A tester system at room temperature. Electrochemical impedance spectroscopy (EIS) was recorded by a Princeton workstation (PARSTAT2273, EG&G, US) over the frequency range from 500 kHz to 10 mHz with an amplitude of 5 mV.

3. Results and discussion

3.1. Characterization of $\text{Na}_2\text{V}_6\text{O}_{16} \cdot 0.14\text{H}_2\text{O}$

Fig. 1 shows the XRD pattern of the as-prepared material. As can be seen, all the diffraction peaks in XRD pattern can be indexed to a monoclinic crystalline $\text{Na}_2\text{V}_6\text{O}_{16} \cdot 3\text{H}_2\text{O}$ phase (JCPDS No. 16-0601) with the lattice parameters $a = 0.9656 \text{ nm}$, $b = 0.3715 \text{ nm}$, $c = 0.7068 \text{ nm}$ and $\beta = 88.62^\circ$. No other diffraction peaks are found, indicating the as-prepared $\text{Na}_2\text{V}_6\text{O}_{16} \cdot 0.14\text{H}_2\text{O}$ is of high purity. It should be pointed out that the strongest diffraction peak (001) shifts toward positive angle and diffraction peaks of (−301), (111) and (−211) move to negative direction, in comparison with the standard card, which is probably due to the removal of some crystal H_2O during the thermal treatment. Such information was stated in our previous work [19]. It was concluded that heat treatment could

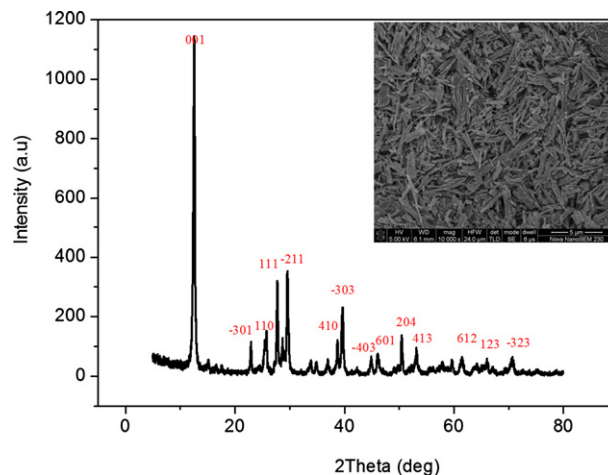


Fig. 1. X-ray diffraction (XRD) pattern of the as-prepared material. The inset is the corresponding SEM image.

greatly improve the cycling stability of the $\text{Na}_2\text{V}_6\text{O}_{16} \cdot x\text{H}_2\text{O}$ mainly due to the removal of the crystal water in the molecule and thus the contraction of crystal volume, although somewhat sacrificing the reversible capacity. The morphology and particle size of the as-prepared material are shown in SEM image (Fig. 1 inset). The as-obtained sample consists of many nanowires with the average length of 2 μm . Some of primary nanowires are partially attached together to form bundles. Actually, some of bundles have large diameter, even up to several micrometers. It is noted that the bundle-morphology consisting of the nanowires could be beneficial for withstanding the volume expanding, thus resulting in the improvement of cycling stability, when the vanadates are used as lithium intercalated materials.

FT-IR measurement was further carried out to verify the existence of the crystal water. The related result is presented in Fig. 2(a). The sample has absorption bands at about 3438.9, 1632.7, 1384.0, 993.6, 951.4, 759.8 and 538.8 cm^{-1} , respectively. Apparently, the bands at 993.6 and 951.4 cm^{-1} are due to V=O stretching of distorted octahedral and distorted square pyramids, while those at 759.8 and 538.8 cm^{-1} are assigned to asymmetric and symmetric stretching vibration of V–O–V bonds, respectively [23]. In addition, there are two another bands at 3438.9 and 1632.7 cm^{-1} , corresponding to crystal H_2O in the as-prepared material [24]. TGA test of the as-prepared material was employed to measure the amount of crystal water. As shown in Fig. 2(b), mass loss of 0.586% between 100 and 400 $^\circ\text{C}$ was observed, which was attributed to the removal

of the crystal water. Accordingly, the amount of crystal water in the sample could be calculated to be about 0.14 per unit. Thus, results above leave no doubt that the as-prepared material is $\text{Na}_2\text{V}_6\text{O}_{16} \cdot 0.14\text{H}_2\text{O}$.

3.2. Electrochemical behavior of $\text{Na}_2\text{V}_6\text{O}_{16} \cdot 0.14\text{H}_2\text{O}$ in Li_2SO_4 with various pH values

It is well known that electrochemical performance of the intercalated materials in aqueous electrolyte depends on the conditions of used electrolyte, particularly the pH values. Therefore, it is of great importance to find proper aqueous electrolyte with the best pH value for $\text{Na}_2\text{V}_6\text{O}_{16} \cdot 0.14\text{H}_2\text{O}$ in order to obtain the optimized aqueous lithium-ion battery. Electrochemical behavior of $\text{Na}_2\text{V}_6\text{O}_{16} \cdot 0.14\text{H}_2\text{O}$ electrode in a saturated Li_2SO_4 (2 M) with various pH values from 7.0 to 12.0 was investigated by cyclic voltammetry (Fig. 3). As observed, each electrode demonstrates one large pair of redox peaks between -0.4 and -0.7 V. Meantime, in the first CV curve, a slight redox shoulder could be found, which is less obvious in the subsequent cycles. The related redox peaks agree well with the lithium-ion insertion/extraction process in an organic electrolyte. The separating of redox peaks in the first cycles can be attributed to the different occupation sites for the lithium ions in the host [25]. Obvious capacity loss in the first 2 cycles could be seen for all cells, which is very common phenomenon for ARLB systems and probably due to the side reactions between Li^+ and aqueous solution, as well as the initial irreversible structure change [18]. It should be pointed out that the difference of the redox potential decreases gradually with the increasing of the electrolyte pH value, consistent with the other reported results for cathode materials [10]. However, increasing pH in this paper results in inferior cycling stability. As for the electrode in neutral Li_2SO_4 , apart from the initial capacity loss, no obvious capacity loss appears in the following curves. On the other hand, large capacity loss is shown for the electrode in Li_2SO_4 with pH 12. Results above imply that $\text{Na}_2\text{V}_6\text{O}_{16} \cdot 0.14\text{H}_2\text{O}$ could be used as lithium reversible intercalated electrode for ARLB and it exhibits the best cycling stability in the neutral solution. It is well proved that not all intercalated electrodes show the best cycling stability in the same pH value. Our group studied the effect of pH to electrochemical stability of $\text{LiNi}_{1/3}\text{Co}_{1/3}\text{Mn}_{1/3}\text{O}_2$ in LiNO_3 solution and chose 5 mol L^{-1} LiNO_3 with pH 11 as the best electrolyte for aqueous lithium-ion battery [26]. Wang and co-workers [27] found that $\text{LiNi}_{1/3}\text{Co}_{1/3}\text{Mn}_{1/3}\text{O}_2$ at Li_2SO_4 solution with pH 13 showed more stability in electrolyte than that with pH 11. Meantime, they considered that capacity fading of the electrode was attributed to H^+ intercalation when cycling in neutral electrolyte [27]. It is noted that increasing the pH value could improve the cycling stability of $\text{LiNi}_{1/3}\text{Co}_{1/3}\text{Mn}_{1/3}\text{O}_2$. However, electrochemical window is thus limited, leading to decreased reversible capacity. With this in mind, a cathode with stable cycling performance in the neutral Li_2SO_4 electrolyte should be employed to construct a high performance ARLB. In fact, studied results indicated that LiFePO_4 and LiMn_2O_4 could keep stable during the lithium insertion/extraction process in the neutral solution, which is different from $\text{LiNi}_{1/3}\text{Co}_{1/3}\text{Mn}_{1/3}\text{O}_2$ [10,28]. Considering its relatively high lithium intercalated potential, commercial LiMn_2O_4 was directly used as cathode. Fig. 4 gives the first 15 cycles of CV curves for LiMn_2O_4 at 0.8 mV s^{-1} in saturated Li_2SO_4 solution. It can be seen that two pairs of redox peaks are located at 0.8 and 0.92 V (versus SCE), which are in accordance with the two-steps of Li-ion de-intercalation/intercalation processes in organic electrolyte. The following 14 CV curves can well repeat the curve shape of the 1st one with no shift of the redox peaks positions, indicating that the electrode is very stable during the lithium insertion/extraction process in a neutral solution. In organic electrolyte, the dissolution

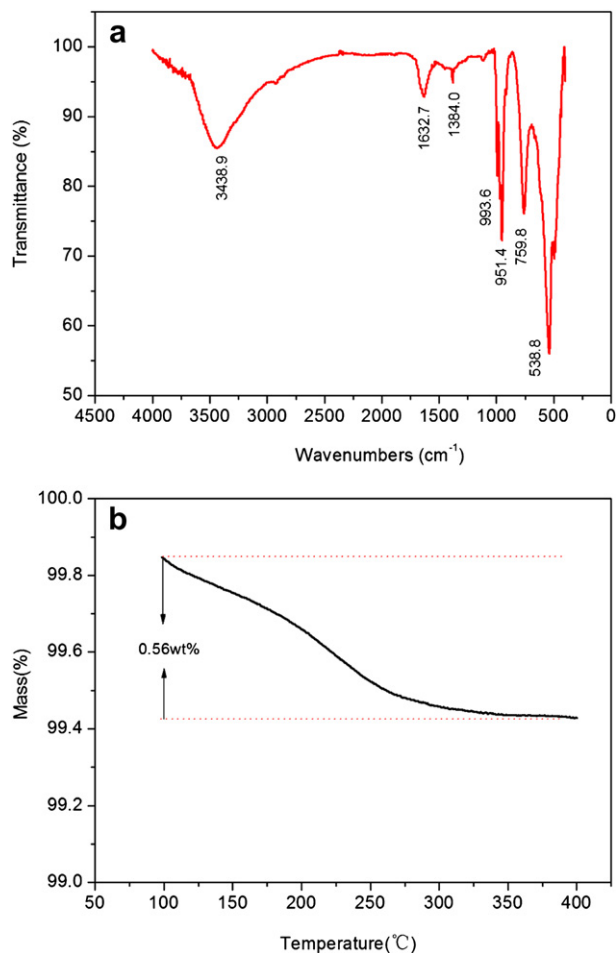


Fig. 2. (a) FT-IR spectrum and TGA curve (b) of the as-prepared $\text{Na}_2\text{V}_6\text{O}_{16} \cdot 0.14\text{H}_2\text{O}$ powder.

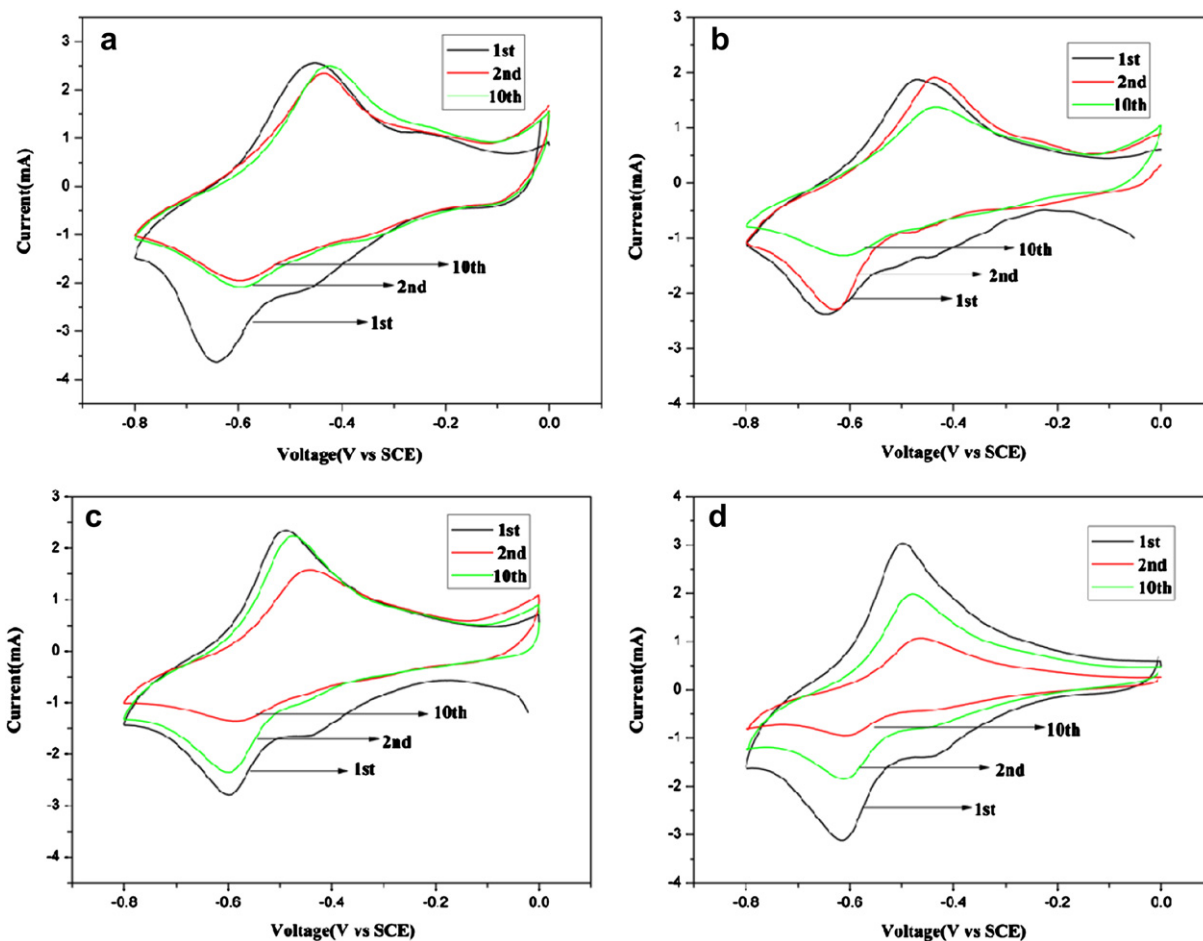


Fig. 3. Cyclic voltammetry curves of $\text{Na}_2\text{V}_6\text{O}_{16} \cdot 0.14\text{H}_2\text{O}$ in a saturated Li_2SO_4 solution with various pH values: (a) pH = 7; (b) pH = 9; (c) pH = 11; (d) pH = 12 between -0.8 and 0 V at a scanning rate of 0.3 mV s^{-1} .

of Mn into the electrolyte is a cause of capacity fade, which resulted by the disproportion reaction: $2 \text{Mn}^{3+} \rightarrow \text{Mn}^{2+} + \text{Mn}^{4+}$ [29]. Similarly, the dissolution of Mn ion also exists in aqueous electrolyte, which is attributed to the polarity of water molecules and no effective membrane formed on the interface between electrode

materials and aqueous electrolyte. However, the ICP-AES result shows that the content of Mn ion dissolved in electrolyte increases by 0.23 wt% from 1 to 50 cycles, which has little effect on capacity fade of the cell. Wang and Xia reported that LiMn_2O_4 can give a very long cycle life of about 10,000 times, which can support our conclusion in certain extent [28,30]. To further investigate the stability of $\text{Na}_2\text{V}_6\text{O}_{16} \cdot 0.14\text{H}_2\text{O}$ and LiMn_2O_4 in aqueous electrolyte, CV curves of $\text{Na}_2\text{V}_6\text{O}_{16} \cdot 0.14\text{H}_2\text{O}$, LiMn_2O_4 and the blank electrode in neutral electrolyte are shown in Fig. 5. As can be seen, except the hydrogen evolution peak at lower than -0.8 V and oxygen evolution at higher than 1.2 V , no other obvious peak was observed in the range of -0.8 to 1.2 V , indicating that the peaks located in the range of -0.8 to 1.2 V are resulted from the active electrode material.

For $\text{Na}_2\text{V}_6\text{O}_{16} \cdot 0.14\text{H}_2\text{O}$, there is one pair of redox peaks at about -0.64 (red) and -0.48 (ox) (versus SCE) in the curve, which is in accordance with the results in Fig. 3.

To estimate the electrochemical performance of $\text{Na}_2\text{V}_6\text{O}_{16} \cdot 0.14\text{H}_2\text{O}$ anode, $\text{Na}_2\text{V}_6\text{O}_{16} \cdot 0.14\text{H}_2\text{O} // \text{LiMn}_2\text{O}_4$ ARLB is fabricated using saturated neutral Li_2SO_4 solution as aqueous electrolyte. CV curve of the studied full cell between 0 and 1.6 V at 0.3 mV s^{-1} is displayed in Fig. 6. There are two obvious oxidation peaks at about $0.87, 1.3 \text{ V}$ and the corresponding reduction peaks at $0.46, 1.18 \text{ V}$. Besides, one pair of weak redox peaks is located at 0.15 V . It is clear that the constructed ARLB shows complicated lithium insertion/extraction behavior. The splitting of many oxidation/reduction peaks is also ascribed to the different lithium sites with energy difference for lithium-ions holding [25].

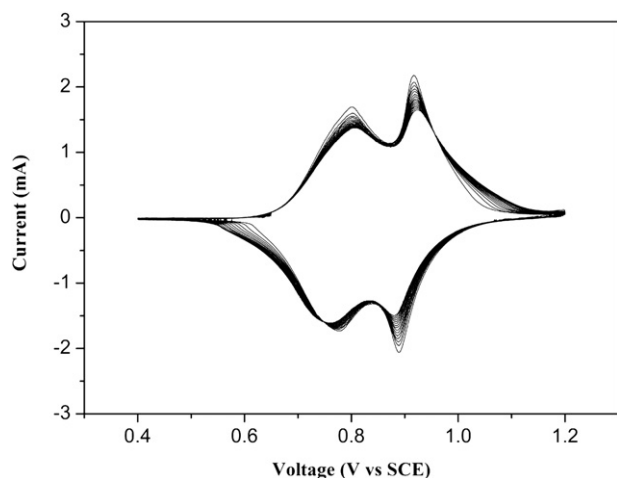


Fig. 4. Cyclic voltammetry curves of LiMn_2O_4 for the first 15 cycles in a saturated Li_2SO_4 aqueous solution, operated between 0.4 and 1.2 V at a scanning rate of 0.8 mV s^{-1} .

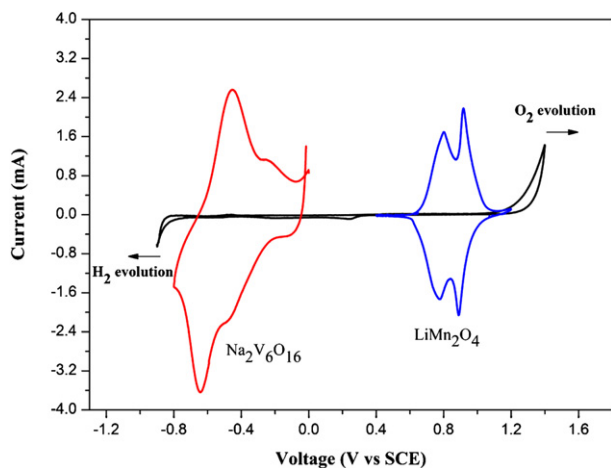


Fig. 5. Linear sweep voltammetry of neutral Li_2SO_4 solution and the first CV curves of $\text{Na}_2\text{V}_6\text{O}_{16} \cdot 0.14\text{H}_2\text{O}$ and LiMn_2O_4 in neutral electrolyte at a scanning rate of 0.3 mV s^{-1} .

3.3. Charge and discharge measurement in aqueous solution

The first discharge curves of $\text{Na}_2\text{V}_6\text{O}_{16} \cdot 0.14\text{H}_2\text{O}/\text{LiMn}_2\text{O}_4$ ARLB in the neutral electrolytes at different current densities are illustrated in Fig. 7. It should be noted that there is no real discharge plateau, which is ascribed to the overlapping of multi-Li-ion de-intercalation/intercalation processes. The initial specific discharge capacity at 60 mA g^{-1} ($1\text{C} = 300 \text{ mA g}^{-1}$) is 122.7 mAh g^{-1} based on the mass of the anode, which is a significant value for the ARLB. If based on the total mass of the anode and cathode, the discharge capacity of this ARLB is about 55.7 mAh g^{-1} (the designing ratio of the anode and cathode is 1:1.2). Although vanadates and their derivative exhibit high capacity (often more than 200 mAh g^{-1}) when used in organic electrolyte, much lower discharge capacities ($40\text{--}100 \text{ mAh g}^{-1}$) can be achieved in aqueous electrolyte even if they are discharged to a low potential close to the H_2 evolution [31,32]. Apparently, the proposed $\text{Na}_2\text{V}_6\text{O}_{16} \cdot 0.14\text{H}_2\text{O}$ electrode shows higher reversible capacity in aqueous solution than most of other vanadates. However, Zhou and co-workers [33] proposed a novel high performance anode material, $\text{H}_2\text{V}_3\text{O}_8$, which delivered a discharge capacity of 234 mAh g^{-1} at 0.1 A g^{-1} in aqueous solution of 5 M LiNO_3 and 0.001 M LiOH . It is obvious that we should focus more attention on improving the reversible capacity of

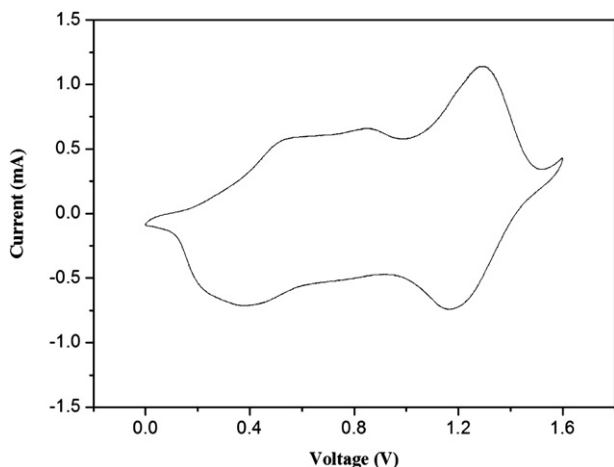


Fig. 6. Cyclic voltammetry curve of $\text{Na}_2\text{V}_6\text{O}_{16} \cdot 0.14\text{H}_2\text{O}/\text{LiMn}_2\text{O}_4$ in a saturated Li_2SO_4 solution, operated between 0 and 1.6 V at a scanning rate of 0.3 mV s^{-1} .

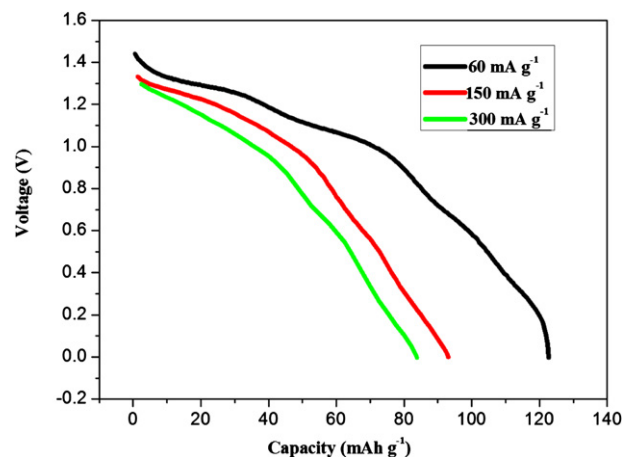


Fig. 7. The initial discharge curves of $\text{Na}_2\text{V}_6\text{O}_{16} \cdot 0.14\text{H}_2\text{O}/\text{LiMn}_2\text{O}_4$ in a saturated Li_2SO_4 solution at different current densities of 60 mA g^{-1} (■), 150 mA g^{-1} (●), 300 mA g^{-1} (▲) between 0 and 1.6 V.

$\text{Na}_2\text{V}_6\text{O}_{16} \cdot 0.14\text{H}_2\text{O}$ in the future work. Note that the initial specific discharge capacities decrease to 94 and 83 mAh g^{-1} when the current densities are increased to 150 and 300 mA g^{-1} , respectively. The rapid capacity loss is attributed to the inferior rate capability of $\text{Na}_2\text{V}_6\text{O}_{16} \cdot 0.14\text{H}_2\text{O}$, which is basically consistent with the rate performance of this material in organic electrolyte [19]. Fig. 8 displays the long cycling performance and charge–discharge curves of $\text{Na}_2\text{V}_6\text{O}_{16} \cdot 0.14\text{H}_2\text{O}/\text{LiMn}_2\text{O}_4$ ARLB at 300 mA g^{-1} . As seen, the ARLB shows excellent cycling stability. In the first 100 cycles, the discharge capacity decays slowly upon the cycling, with the capacity retention of 96.9%, 88% after 20 and 50 cycles, respectively. It is worth pointing out that no obvious capacity fading is observed in the later 100 cycles, which also can be seen from the curves in Fig. 8(b). After 100 and 200 cycles, the capacity retention is 80.1%, 77%, respectively. The cycling performance of this ARLB using $\text{Na}_2\text{V}_6\text{O}_{16} \cdot 0.14\text{H}_2\text{O}$ is much better than most ARLB systems using vanadates, such as $\text{VO}_2(\text{B})$, $\text{Li}_x\text{V}_2\text{O}_5$, LiV_3O_8 [4,17,18,34]. $\text{VO}_2(\text{B})/\text{LiMn}_2\text{O}_4$ can be cycled only for 25 cycles as reported by Dahn and co-workers [4]. The capacity retention of $\text{Li}_x\text{V}_2\text{O}_5/\text{LiMn}_2\text{O}_4$ is only 8% of the original capacity after 40 cycles [17]. When LiV_3O_8 was used as anode, the cycling stability of the ARLB was improved, but is still far insufficient for practical application. $\text{LiV}_3\text{O}_8/\text{LiCoO}_2$ exhibited the capacity retention of 65% after 40 cycles [34], while $\text{LiV}_3\text{O}_8/\text{LiNi}_{0.81}\text{Co}_{0.19}\text{O}_2$ showed 70% of the initial capacity after 30 cycles and 25% after 100 cycles [18], respectively. Considering the complicated Li^+ insertion/extraction process between the active materials and the aqueous electrolyte, the pristine anode material often suffer from large structure transformation, thus resulting in significant capacity loss. Accordingly, appropriate coating strategies have been widely employed to further enhance the cycling performance of ARLB. Note that the used $\text{Na}_2\text{V}_6\text{O}_{16} \cdot 0.14\text{H}_2\text{O}$ electrode here is without any coating layer. There is no doubt that the $\text{Na}_2\text{V}_6\text{O}_{16} \cdot 0.14\text{H}_2\text{O}$ electrode here exhibits good cycling stability. It is believed that such electrode could be used as a very promising anode material for ARLB.

With regard to the poor cyclic stability of above ARLB systems, probable capacity fade mechanisms of aqueous lithium-ion battery have been proposed by some research groups and are mainly focused on the metal ion dissolution in aqueous solution, structural changes of electrode materials, as well as the decomposition of water and so on. It is reported that decomposition of water in aqueous electrolyte often results in relatively low Coulombic efficiency [35]. In this paper, the overall average Coulombic efficiency of $\text{Na}_2\text{V}_6\text{O}_{16} \cdot 0.14\text{H}_2\text{O}/\text{LiMn}_2\text{O}_4$ is around 92% at 300 mA g^{-1} , which

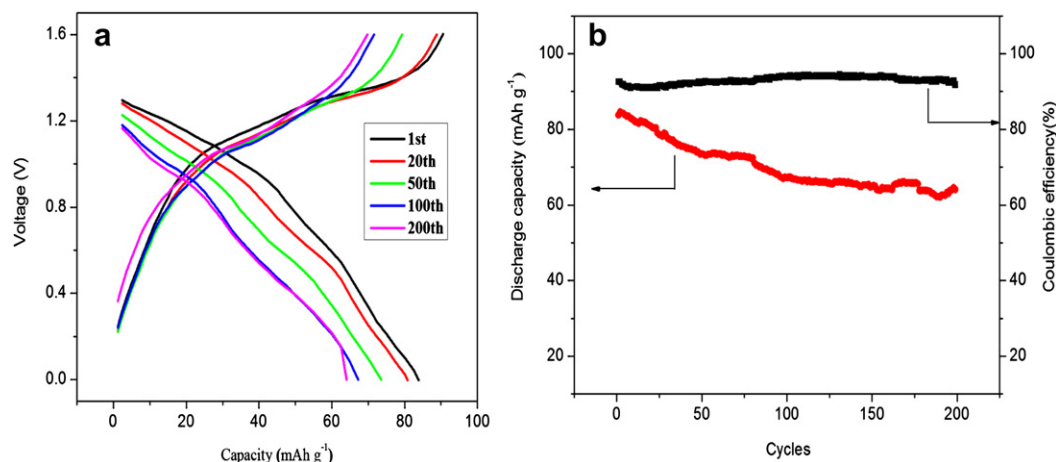


Fig. 8. (a) Charge and discharge curves for different cycles of $\text{Na}_2\text{V}_6\text{O}_{16} \cdot 0.14\text{H}_2\text{O} // \text{LiMn}_2\text{O}_4$ at 300 mA g^{-1} between 0 and 1.6 V; (b) The corresponding discharge capacity and Coulombic efficiency versus cycle numbers.

is much higher than that (75%) of VO_2 (B) [4]. The good cycling stability of $\text{Na}_2\text{V}_6\text{O}_{16} \cdot 0.14\text{H}_2\text{O} // \text{LiMn}_2\text{O}_4$ should be probably attributed to the stable anode and the suppressed decomposition of the water. More work relating to further improving the reversible capacity and the cycling performance by the coating strategies or optimizing the cell designing is now in progress in our group.

To further investigate the possible explanations for excellent cycling stability of $\text{Na}_2\text{V}_6\text{O}_{16} \cdot 0.14\text{H}_2\text{O} // \text{LiMn}_2\text{O}_4$ ARLB, Nyquist plots of the full cell in the charge state of 1.0 V after different cycles (3rd and 100th) at 300 mA g^{-1} are collected and given in Fig. 9. As shown, each impedance spectrum consists of a depressed semicircle at the high-medium frequency followed by a slope line at the low frequency range. The depressed semicircle is attributed to charge-transfer impedance, while the slope line is due to Warburg impedance which reflects lithium-ion diffusion in the solid state electrodes [36,37]. For comparison, no obvious change has happened in both impedance spectra after different cycles, particularly the charge-transfer impedance. In some previous reports, change of charge-transfer resistance was considered as the important factor to capacity fading for cathode materials [38,39]. Sun and co-workers [38] considered that the improved electrochemical performance of AlF_3 -coated LiCoO_2 could be explained by

the lower charge-transfer resistance (R_{ct}) and reduced Co dissolution of the coated electrode. Li and co-workers [39] concluded that $\text{LiNi}_{0.5}\text{Mn}_{0.4}\text{Co}_{0.1}\text{O}_2$ with improved rate capabilities, compared with non-doped $\text{LiNi}_{0.5}\text{Mn}_{0.5}\text{O}_2$ was attributed to the decrease in charge-transfer resistance. EIS results indicate that the charge-transfer impedance keeps stable during long cycling test, which agrees with the good cycling performance in Fig. 8. Considering that the charge-transfer impedance in Fig. 9 involves the contributions from cathode and anode, we still have no enough evidence to show which part is more important. But one thing can be sure that the contribution from $\text{Na}_2\text{V}_6\text{O}_{16} \cdot 0.14\text{H}_2\text{O}$ anode is very small since the total resistance change is not apparent. More research work will be carried out in our group to explain why the $\text{Na}_2\text{V}_6\text{O}_{16} \cdot 0.14\text{H}_2\text{O} // \text{LiMn}_2\text{O}_4$ ARLB exhibits such good cycling stability.

4. Conclusion

As a novel anode material, $\text{Na}_2\text{V}_6\text{O}_{16} \cdot 0.14\text{H}_2\text{O}$ nanowires were first proposed for aqueous lithium-ion battery. CV results showed that the as-prepared material had good reversible lithium-ion insertion/extraction process in neutral Li_2SO_4 . ARLB of $\text{Na}_2\text{V}_6\text{O}_{16} \cdot 0.14\text{H}_2\text{O} // \text{LiMn}_2\text{O}_4$ was constructed and showed good electrochemical performance, in terms of high discharge capacity and good cycling stability. At 60 mA g^{-1} , the ARLB exhibited an initial discharge capacity of 122.7 mAh g^{-1} on the basis of the mass of anode material. When the current density was up to 300 mA g^{-1} , discharge capacity of 83 mAh g^{-1} remained with the capacity retention of 77% over 200 cycles. No considerable increasing of charge-transfer impedance was discovered from the EIS results. There is no doubt that the annealed $\text{Na}_2\text{V}_6\text{O}_{16} \cdot 0.14\text{H}_2\text{O}$ nanowires with good structure stability would be significantly beneficial to improvement of the cycling performance for as-studied ARLB.

Acknowledgments

Financial support from the National Natural Science Foundation of China (No. 51072234 and No. 20971129), the Postdoctoral Science Foundation of Central South University and Scientific Research Foundation of Central South University is greatly appreciated.

References

- [1] M. Armand, J.M. Tarascon, *Nature* 451 (2008) 652–657.
- [2] H.Y. Wang, K.L. Huang, C.H. Huang, S.Q. Liu, Y. Ren, X.B. Huang, *J. Power Sources* 196 (2011) 5645–5650.

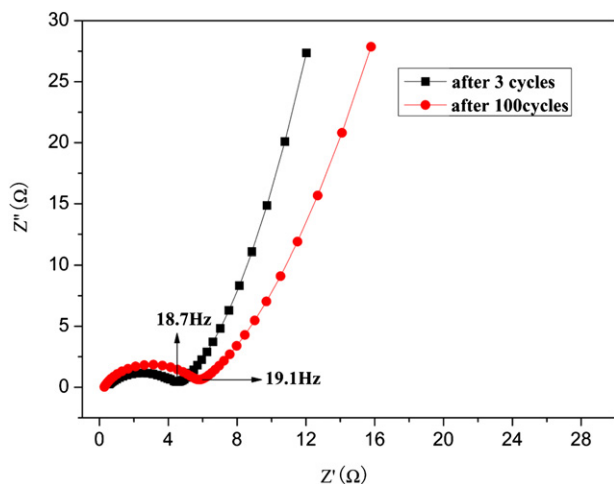


Fig. 9. Nyquist plots of $\text{Na}_2\text{V}_6\text{O}_{16} \cdot 0.14\text{H}_2\text{O} // \text{LiMn}_2\text{O}_4$ at 1.0 V after 3 and 100 cycles at 300 mA g^{-1} .

- [3] H.Y. Wang, Y. Ren, Y. Wang, W.J. Wang, S.Q. Liu, *Cryst. Eng. Commun.* 14 (2012) 2831–2836.
- [4] W. Li, J.R. Dahn, D. Wainwright, *Science* 264 (1994) 1115–1118.
- [5] G. James, *Science* 264 (1994) 1084.
- [6] J.Y. Luo, Y.Y. Xia, *Adv. Funct. Mater.* 17 (2007) 3877–3885.
- [7] C. Wessells, R.A. Huggins, Y. Cui, *J. Power Sourc.* 196 (2011) 2884–2888.
- [8] A. Caballero, J. Morales, O.A. Vargas, *J. Power Sourc.* 195 (2010) 4318–4321.
- [9] G.J. Wang, L.J. Zhang, L.J. Fu, B. Wang, Y.P. Wu, *Electrochem. Commun.* 9 (2007) 1873–1876.
- [10] J.Y. Luo, W.J. Cui, P. He, Y.Y. Xia, *Nat. Chem.* 2 (2010) 760–765.
- [11] R. Ruffo, C. Wessells, R.A. Huggins, Y. Cui, *Electrochem. Commun.* 11 (2009) 247–249.
- [12] G.J. Wang, L.J. Fu, B. Wang, N.H. Zhao, Y.P. Wu, R. Holze, *J. Appl. Electrochem.* 38 (2008) 579–581.
- [13] P. He, X. Zhang, Y.G. Wang, L. Cheng, Y.Y. Xia, *J. Electrochem. Soc.* 155 (2008) A144–A150.
- [14] Y. Xu, X.S. Han, L. Zheng, S.Q. Wei, Y. Xie, *Dalton Trans.* 40 (2011) 10751–10757.
- [15] Y. Xu, L. Zheng, C.Z. Wu, F. Qi, Y. Xie, *Chem. Eur. J.* 384 (2011) 384–391.
- [16] G.J. Wang, Q.T. Qu, B. Wang, Y. Shi, S. Tian, Y.P. Wu, R.J. Holze, *J. Power Sourc.* 189 (2009) 503–506.
- [17] H.B. Wang, Y.Q. Zeng, K.L. Huang, S.Q. Liu, L.Q. Chen, *Electrochim. Acta* 52 (2007) 5102–5107.
- [18] J. Kohler, H. Makiyara, H. Uegaito, H. Inoue, M. Toki, *Electrochim. Acta* 46 (2000) 59–65.
- [19] H.Y. Wang, W.J. Wang, Y. Ren, K.L. Huang, S.Q. Liu, *J. Power Sourc.* 199 (2012) 263–269.
- [20] Y. Xu, X.S. Han, L. Zheng, W.S. Yan, Y. Xie, *J. Mater. Chem.* 21 (2011) 14466–14472.
- [21] M.E. Spahr, P. Novák, W. Scheifele, O. Haas, R. Nesper, *J. Electrochem. Soc.* 145 (1998) 421–427.
- [22] H.Y. Wang, S.Q. Liu, Y. Ren, W.J. Wang, A.D. Tang, *Energy Environ. Sci.* 5 (2012) 6173–6179.
- [23] B. Azambre, M.J. Hudson, O. Heintz, *J. Mater. Chem.* 13 (2003) 385–389.
- [24] L.Q. Mai, C.S. Lao, B. Hu, J. Zhou, Y.Y. Qi, W. Chen, E.D. Gu, Z.L. Wang, *J. Phys. Chem. B* 110 (2006) 18138–18141.
- [25] J. Kawakita, M. Majima, T. Miura, T. Kishi, *J. Power Sourc.* 66 (1997) 135–139.
- [26] H.B. Wang, K.L. Huang, Y.Q. Zeng, L.Q. Chen, *Electrochem. Solid State Lett.* 10 (2007) A199–A203.
- [27] Y.G. Wang, J.Y. Luo, C.X. Wang, Y.Y. Xia, *J. Electrochem. Soc.* 153 (2006) A1425–A1431.
- [28] Y.G. Wang, Y.Y. Xia, *J. Electrochem. Soc.* 153 (2006) A450–A454.
- [29] Q.T. Qu, L.J. Fu, X.Y. Zhan, D. Samuelis, J. Maier, L. Li, S. Tian, Z.H. Li, Y.P. Wu, *Energy Environ. Sci.* 4 (2011) 3985–3990.
- [30] Y.G. Wang, Y.Y. Xia, *Electrochem. Commun.* 7 (2005) 1138–1142.
- [31] M.S. Zhao, Q.Y. Zheng, F. Wang, W.M. Dai, X.P. Song, *Electrochim. Acta* 56 (2011) 3781–3784.
- [32] Y. Xu, L. Zheng, Y. Xie, *Dalton Trans.* 39 (2010) 10729–10738.
- [33] H.Q. Li, T.Y. Zhai, P. He, Y.G. Wang, E. Hosono, H.S. Zhou, *J. Mater. Chem.* 21 (2011) 1780–1787.
- [34] G.J. Wang, L.J. Fu, N.H. Zhao, L.C. Yang, Y.P. Wu, H.Q. Wu, *Angew. Chem. Int. Ed.* 119 (2007) 299–301.
- [35] H.B. Wang, K.L. Huang, Y.Q. Zeng, S. Yang, L.Q. Chen, *Electrochim. Acta* 52 (2007) 3280–3285.
- [36] Y.J. Kang, J.H. Kim, S.W. Lee, Y.K. Sun, *Electrochim. Acta* 50 (2005) 4784–4791.
- [37] F. Nobili, F. Croce, B. Scrosati, R. Marassi, *Chem. Mater.* 13 (2001) 1642–1646.
- [38] Y.K. Sun, J.M. Han, S.T. Myung, S.W. Lee, K. Amine, *Electrochem. Commun.* 8 (2006) 821–826.
- [39] D.C. Li, Y.K. Sasaki, K. Kobayakawa, Y.C. Sato, *J. Power Sourc.* 157 (2006) 488–493.